

Egalitarianism among Bubbles in Porous Media: An Ostwald Ripening Derived Anticoarsening Phenomenon

Ke Xu,^{1,*} Roger Bonnecaze,² and Matthew Balhoff^{1,†}

¹*The Hildebrand Department of Petroleum and Geosystems Engineering,
The University of Texas at Austin, Austin, Texas 78712, USA*

²*McKetta Department of Chemical Engineering and Texas Materials Institute,
The University of Texas at Austin, Austin, Texas 78712, USA*

(Received 15 May 2017; revised manuscript received 5 September 2017; published 29 December 2017)

We show that smaller gas bubbles grow at the expense of larger bubbles and all bubbles approach the same surface curvature after long times in porous media. This anticoarsening effect is contrary to typical Ostwald ripening and leads to uniformly sized bubbles in a homogeneous medium. Evolution dynamics of bubble populations were measured, and mathematical models were developed that fit the experimental data well. Ostwald ripening is shown to be the driving mechanism in this anticoarsening phenomenon; however, the relationship between surface curvature and bubble size determined by the pore-throat geometric confinement reverses the ripening direction.

DOI: 10.1103/PhysRevLett.119.264502

Coarsening of particles, drops, and bubbles, or Ostwald ripening [1] is a well-known phenomenon that occurs in two-phase or multiphase mixtures such as foam and emulsions [2–4] and in nanoparticles synthesis processes [5–7]. During an Ostwald ripening process in an open system, the gas in small bubbles, for example, dissolves in the surrounding fluid and diffuses to larger bubbles to grow them. This mass transfer is driven by higher capillary pressure or chemical potential of the gas in the small bubbles relative to that in the larger bubbles. Ostwald ripening reduces the surface energy. Lifshitz and Slyozov [8] proposed a theory of a steady-state growth regime with the average cluster size R increasing in time following $R \propto t^\alpha$ ($\alpha \in [0, 1]$), which was further improved by others [9–16].

Theories proposed to quantify the kinetics of the evolution of bubble size during Ostwald ripening are based on an assumption of an open system, where bubbles or other particulate phases (i.e., droplets, particle clusters) can grow freely without any restriction from a closed boundary and/or geometric confinement [9,16,17]. A few experiments and simulations have shown that geometric confinement does affect the dynamics of Ostwald ripening. Numerical simulations reported [18,19] for a two-dimensional (2D) fiber-shaped channel network, specifically representing the Vycor glass structure, showed that the Ostwald ripening slows down considerably, although no direct experimental evidence were available. Huang *et al.* [20] recently showed experimental results that 2D arrays of micropillars can limit the growth of bubbles, although no quantitative comparison to a model were provided to describe the evolution of the bubbles.

In nature and industrial applications, one of the most common geometric confinements are micron-scale 3D porous media consisting of interconnected pores segregated

by solid grains, as appears in soils, rocks, packed beds, and many membrane systems, where pore bodies with relatively larger sizes and throats with relatively smaller sizes are periodically distributed. Ostwald ripening in such a geometry is significant for understanding the distribution of nonaqueous phase liquid (NAPL) pollutants in soil and aquifer systems [21], enhanced oil recovery (EOR) [22,23], flow in fuel cell membranes [24], and CO₂ storage in underground strata of porous rock [25,26], where bubbles and droplets are confined and trapped in pores due to large capillary forces.

Here we show that the evolution of the size of bubbles in a micron-scale porous medium is very different from that in an open system. Unlike the coarsening typically observed in open systems, an initially polydisperse population of bubbles will ultimately become monodisperse and there is egalitarianism in bubble size for sufficient confinement in a homogenous porous medium, with gas from the larger bubbles diffusing to smaller bubbles. Experimental measurements of the size distribution and curvatures of the bubbles were conducted on a glass micromodel, and a theoretical model was developed that accurately predicts the dynamics of individual bubbles and evolution of the bubble population towards a uniform size.

In an open system [Fig. 1(a)], there is a positive feedback between the bubble size and the bubble growth rate. Governed by the Laplace equation (the capillary $P_c = \gamma\kappa$, where κ is the curvature of bubble surface and γ is the surface tension), a growing bubble has decreasing surface curvature, leading to decreasing capillary pressure and lower chemical potential for the gas, which increases the driving force to further grow the bubble from smaller ones. However, in a porous medium, geometric confinement can reverse this feedback. As shown in Fig. 1(b), when a bubble is large

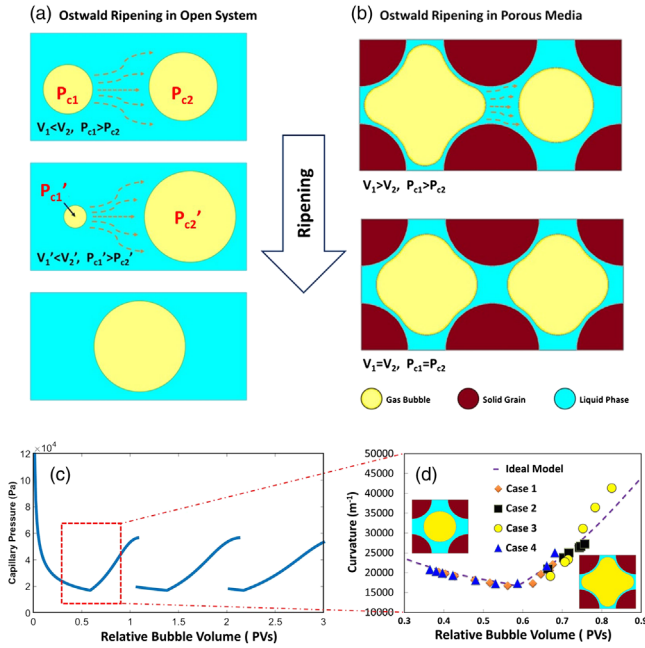


FIG. 1. (a) Schematic of typical Ostwald ripening in an open system. Driven by the capillary pressure difference gas molecules diffuse from a smaller bubble with high gas pressure to a larger one with lower pressure, until the small bubble disappears. (b) Ostwald ripening in homogeneous porous media. Because of the geometric confinement, the larger bubble can have a larger capillary pressure than the smaller one, driving gas molecules from the larger bubble to smaller one, until they reach the same shape and capillary pressure. (c) Sketch of the relationship between relative bubble volume and curvature in a 2D array, which is nonlinear. (d) Curvatures measured from experiments compared to that predicted by the 2D model presented in this Letter. The curvatures are measured during the ripening process. Case 1–4 represent the size-curvature relationship during the ripening of 4 different bubbles, as described in Supplemental Material [27].

enough to be deformed by the solid grain, the capillary pressure would increase, rather than decrease, with an increase in droplet size. Figure 1(c) shows a typical relationship between relative bubble volume (defined as the ratio of bubble volume to pore volume) and surface curvature (which is proportional to capillary pressure) in a 2D medium, with circular grains with diameters of $165 \mu\text{m}$ and throats with widths of $35 \mu\text{m}$. The bubble is assumed at rest and the internal and external pressures are in equilibrium. The capillary pressure does not decrease monotonically with the volume of the bubble. Near one pore volume, capillary pressure is at a minimum when the bubble edge just contacts the surfaces of the grains. Above this size bubbles of varying volumes are shown to have almost linearly increasing curvature as they become larger and are constrained by the surrounding porous medium [Fig. 1(d)]. A similar trend is also observed when the bubble is larger than one pore volume. Thus, a larger bubble can have a larger capillary pressure than smaller bubbles, leading to gas molecular diffusion from larger bubbles to smaller bubbles, until they

achieve the same capillary pressure. For the simple two-bubble case shown in Fig. 1(b), those two bubbles eventually reach the same size.

In order to validate this hypothesis, a homogeneous, 2.5D glass micromodel [30] was fabricated to observe bubble evolution in porous media. The micromodel consists of a periodic 2D array of grains and pores, but with the local depth of the throats being shallower than the pores. This introduces a key 3D feature that allows for capillary snap off not seen in typical 2D micromodels. The depth of the pore body h is $26.4 \pm 1 \mu\text{m}$, the grain diameter is $165 \mu\text{m}$, the distance between the centers of two neighboring grains D_l is $200 \mu\text{m}$, and the width of throat (at the narrowest cross section) is $35 \mu\text{m}$.

Deionized (DI) water (surface tension $\gamma = 71.2 \text{ mN/m}$) and surfactant aqueous solutions (0.005 wt % with $\gamma = 35.1 \text{ mN/m}$ and 0.1 wt % TX-100 with $\gamma = 25.4 \text{ mN/m}$) are used as aqueous phases. Liquid phases are dyed for clearer visualization. Air was applied as the gaseous phase. The experimental pressure is 1 atm. Bubbles are generated by coinjection of two phases into the porous medium and gas being trapped in the pore bodies due to the capillary pressure. Several microscopic images were taken over several days, during which the size distribution of the bubbles evolves. Bubble sizes and curvature are captured from microscopic images.

Details of the micromodel fabrication and characterization, flow experimental operation, and image analysis methods are described in the Supplemental Material [27].

A confirmatory experiment was conducted with a surfactant stabilized gas-in-water system. Microscopic images at time 0 and after 120 h of ripening are shown in Fig. 2. Initially, both small and large bubbles are observed. However, after 120 h of ripening, the size distribution of bubbles becomes narrower. The statistics of bubble sizes are shown in Fig. 3. The size distribution of bubbles is initially wide: about 30% of bubbles are smaller than 60% of one pore volume, and about 20% are larger than 80% of one pore volume. After 120 h of ripening, more than 97% of the volumes of all bubbles fall in the interval of 60% to 80% of one pore volume. These results agree with our hypothesis of confinement causing large bubbles to shrink to grow the smaller bubbles, contrary to the coarsening effect observed in open systems.

A mathematical model of the bubble size distribution dynamics was developed to better understand and predict this anticoarsening effect in porous media. In order to achieve a simplified but useful model, we assume the following: (i) The porous medium is homogeneous. (ii) The average bubble volume is larger than the maximum volume of a spherical bubble that can fit in the pore body (critical volume, at which volume the capillary pressure is at a minimum). This is always true according to previous observations in micromodels [31] and in our experiment. It should be noted that existence of very small bubbles may

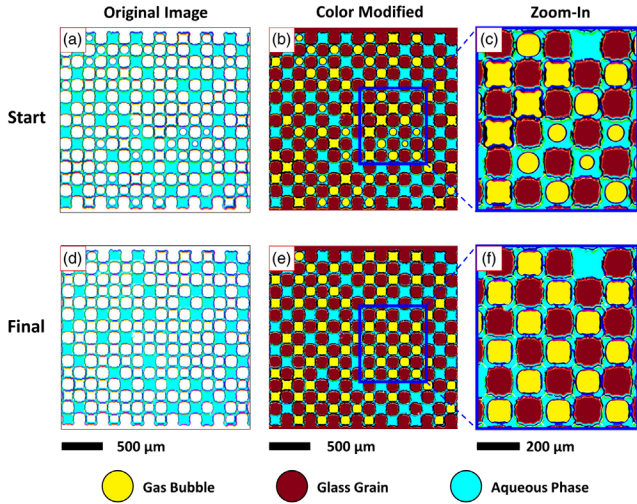


FIG. 2. Evolution of bubble sizes at two different times. (a)–(c) Microscopic image, color-modified image, and close up of color-modified image of the bubble-in-water system in micro-model at time 0. (d)–(f) Microscopic image, color-modified image, and close up of color-modified image of the bubble-in-water system after ripening for 120 h. Images in the same column share the same scale bars. The brown regions are grains, blue regions are filled with aqueous phase, and the yellow regions are bubbles.

make the average bubble volume smaller than the critical volume; however, some of those very small bubbles can disappear in a relatively short time due to classical Ostwald ripening with volume transferred to other bubbles, which finally brings the average bubble volume above the critical volume, as shown in supplemental experiments and discussion presented in the Supplemental Material [27]. (iii) There is no more than one bubble in one pore. If there is no strong interfacial stabilizer [32] to prevent coalescence, this assumption is likely to hold after flow is ceased. (iv) One bubble occupies no more than one pore. This assumption holds if capillary snap-off can occur (which is always true in 3D porous media and in this 2.5D micromodel [30]), or after adequate shearing and pinching on droplet or bubbles when flowing in porous media [31,33–36]. (v) The total number of bubbles is constant during the experiment. As very small droplets will dissolve into the liquid in very short time, the existence of those bubbles can be neglected if the ripening time is on a much longer time scale. (vi) Total gas volume is constant, with no flow and no gravity effect.

Based on above assumptions, we derived analytical models for both single bubble ripening dynamics and for bubble population ripening dynamics. Detailed derivations are presented in the Supplemental Material [27], and a brief framework is shown in the following paragraphs.

As a first order approximation, we only consider the interaction between neighboring bubbles to model the evolution of a single bubble. Similar to the Ostwald ripening in an open system, the difference in capillary

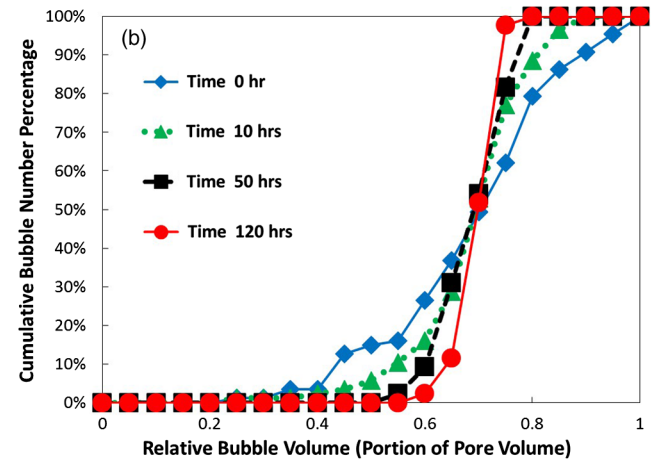
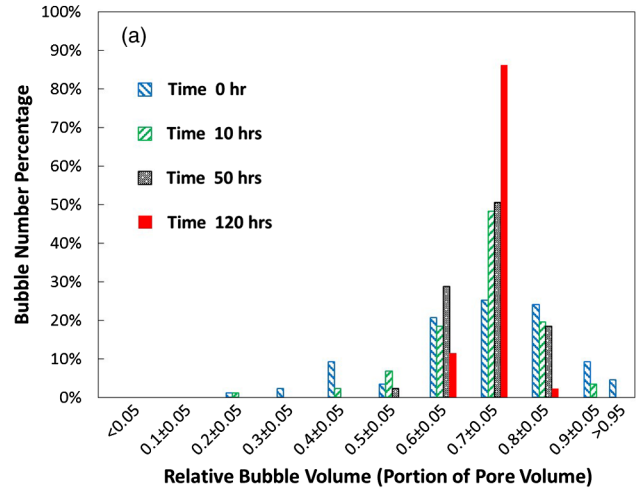


FIG. 3. Evolution of bubble size distribution from the experiment in Fig 2. (a) The percentage of bubbles falling into different volume intervals, after ripening for 0, 12, 60, and 120 h. (b) The cumulative bubble volume distribution curves, after ripening for 0, 12, 60, and 120 h.

pressure is the driving force. Thus, a single bubble's volume change rate should be proportional to the average difference of capillary pressure between a bubble and its neighbors ($\overline{\Delta P_c}$), defined as

$$\overline{\Delta P_c} = \frac{1}{n} \sum (P_{c,i} - P_{c,0}), \quad (1)$$

where n is the number of neighboring bubbles of the specified bubble, $P_{c,0}$ is the capillary pressure of the specified bubble monitored, and $P_{c,i}$ is the capillary pressure of a neighboring bubble, i . Based on Fick's law of diffusion and Henry's law of gas-distribution equilibrium, we find that the dynamics of growth or shrinking of a single bubble in a porous media is given by

$$\frac{dV}{dt} = kn \frac{\overline{\Delta P_c}}{\bar{l}}, \quad \text{where } k \approx \frac{\rho_{\text{liq}} M_{\text{gas}} A_{\text{cross}} D_{\text{gas-liq}}}{\rho_{\text{gas}} M_{\text{liq}} K^{px}}. \quad (2)$$

\bar{l} is the average mass transfer distance between the specific bubble and its neighboring bubbles, ρ_{liq} and ρ_{gas} are the densities of liquid phase and gas phase, respectively, M_{gas} and M_{liq} are the molecular weight of the gas phase and liquid phase, respectively, A_{cross} is the average effective cross section of the diffusion pathway, $D_{\text{gas-liq}}$ is the gas diffusion coefficient in the liquid, and K^{px} is the Henry's law volatility constant defined as the ratio of gas phase pressure divided by gas molar ratio in the aqueous phase. Small amount of surfactant, bubble size distribution, and phase ratio do not affect k . Clearly, larger interfacial tension, smaller distance between two pores, better connectivity can accelerate ripening on a specific bubble.

It is useful to define an appropriate statistical indicator to characterize the bubble volume distribution. Here we introduce U , the half total absolute deviation, which is defined as

$$U = \frac{1}{2} \sum |V_i - V_{\text{av}}|, \quad (3)$$

where V_i is the volume of bubble i , V_{av} is the average bubble volume in the system. We chose U as a distribution indicator because of its clear physical meaning: U is the minimum amount of gas to diffuse globally in order to achieve monodisperse bubbles.

By summing the ripening dynamics of all individual bubbles [Eq. (2)] to describe the evolution of U , combined with some linear approximations, we finally find the ripening dynamics of a bubble population is given by

$$U = U_0 \exp\left(-\frac{1}{\mu_{\text{eq}}} \frac{n_{\text{av}} \gamma}{l_0} t\right), \quad (4)$$

where U_0 is the value of U at time 0, μ_{eq} is a constant determined by fluid properties and the porous medium geometry, with no relationship to operational parameters. n_{av} is defined as the average neighboring bubbles number of a bubble in this system, which is estimated by single pore volume, V_{pore} , the gas saturation S_g , V_{av} , and average pore connectivity n as $n_{\text{av}} \approx (V_{\text{pore}}/V_{\text{av}}) S_g n_0$. l_0 is the mass transfer distance between the surfaces of two bubbles in neighboring pores (which could also be defined as the length of a throat). It should be noted that Eq. (4) is a completely theoretical model, and all parameters in Eq. (4) can be directly measured or estimated from the geometry of porous media and fluid properties before getting any ripening data, and without any empirical constants.

In order to validate these derived models, five independent experiments were conducted on the same micromodel. Key parameters are shown in Table I. During the experiments, all listed assumptions were observed valid. Bubble size distribution data and the validation of single-bubble ripening model [Eq. (2)] is shown in the Supplemental Material [27].

TABLE I. Parameters for five experiments.

	Expt.1	Expt.2	Expt.3	Expt.4	Expt.5
γ (mN/m)	71.2	25.4	25.4	35.1	35.1
S_g	0.700	0.396	0.440	0.581	0.696
U_0 (PVs)	4.74	2.99	2.66	3.54	5.70
$V_{\text{av}}/V_{\text{pore}}$ (PVs)	0.802	0.699	0.705	0.766	0.834

Figure 4 show the evolution of the bubble population during ripening process from experiments, compared to the theoretical model. The time evolutions of U for five independent experiments are shown in Fig. 4(a). A deceleration in ripening rate is observed. As shown in Fig. 4(b), all data from five independent experiments collapse onto one curve, with the unified scale factor (by fitting) $\mu_{\text{eq}} = 2.8 \times 10^7$ Pa s, which closely matches our theoretical prediction of μ_{eq} (3.2×10^7 Pa s). The prediction of μ_{eq} is shown in the Supplemental Material

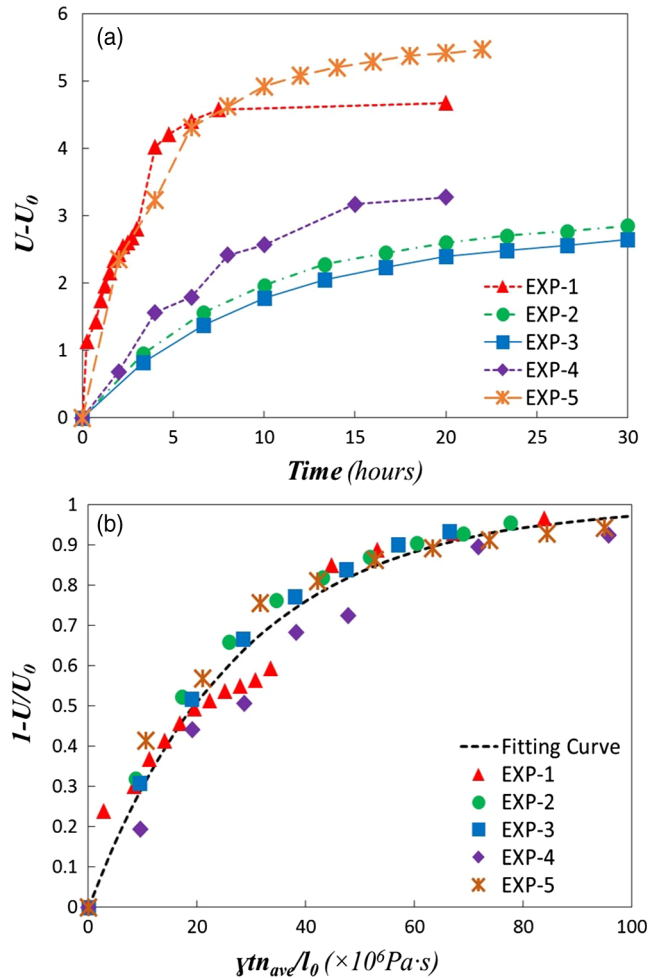


FIG. 4. Modeling of bubble population ripening dynamics. (a) The evolution of $U_0 - U$ for five experiments, where those five sets of data follow different curves. (b) Fitting of five sets of data against Eq. (4), where the evolution curves of five experiments collapse into one.

[27]. The excellent matching between the model predictions and experimental observations validates Eq. (4).

In summary, we show that the direction of Ostwald ripening of bubbles is reversed in porous media due to confinement. Under certain circumstances, the system can even achieve egalitarianism among the bubbles in terms of their size. That is, gas bubbles with a wide size distribution trapped in a porous medium will evolve into a monodisperse size distribution. This anticoarsening effect is driven by the capillary pressure difference, and directed by the micron-scale geometric confinement. The evolution dynamics on bubble population is described by Eq. (4), which is a completely theoretical with no empirical parameters. Experiments conducted on a 2.5D micromodel proved those ripening dynamics models, with the bubble population evolution dynamics model match the experimental data well.

Based on our experiments and models, this anticoarsening effect significantly changes the bubble size distribution in tens of hours. Thus, understanding this anticoarsening effect of bubbles or droplets in porous media is of great significance for better description and operations in many applications which involve time scales similar to or longer than several hours, such as underground storage of carbon dioxide (decades to centuries), the formation and concentration of oil and gas in reservoirs (millions of years), transport of NAPLs in soil (days or even years), and foam-based enhanced oil recovery (months to years).

However, it should be noted that the model presented here is for idealized homogeneous porous media, so the modifications of those models should be introduced when heterogeneity occurs. In addition, if there are a significant number of bubbles larger than one pore volume without snap off, the monodisperse bubbles will not be achieved. When flow occurs, all diffusion related calculations must be rederived. All those problems should be analyzed in future work. Regardless, the conclusion that geometric pore-throat confinement will drive all survived bubbles towards identical capillary pressure (i.e., identical surface curvature at free interfaces) is applicable to multiphase behavior in underground aquifers, hydrocarbon reservoirs, fuel cell systems, and the deep stratum for CO₂ storage hydrocarbon reservoirs, when the capillary forces are dominant.

We gratefully acknowledge support from the sponsors of the Nanoparticles for Subsurface Engineering Industrial Affiliates Program at the University of Texas at Austin (Baker Hughes, a GE Company, Nissan Chemical America, Foundation CMG). We thank Dr. Chun Huh and Dr. Hugh Daigle for their encouragement and support in this research. Dr. Peixi Zhu, Dr. Ayaz Mehmani, Mr. Pengpeng Qi, Ms. Yujing Du, and Mr. Lucas Mejia are acknowledged for their help in micromodel fabrications.

*thuk-xu08@utexas.edu

†balhoff@mail.utexas.edu

[1] P. W. Voorhees, *J. Stat. Phys.* **38**, 231 (1985).

- [2] M. B. Meinders and T. van Vliet, *Adv. Colloid Interface Sci.* **108–109**, 119 (2004).
- [3] A. J. Markworth, *Metallography* **3**, 197 (1970).
- [4] A. J. Markworth, *J. Colloid Interface Sci.* **107**, 569 (1985).
- [5] H. G. Yang and H. C. Zeng, *J. Phys. Chem. B* **108**, 3492 (2004).
- [6] N. V. Mantzaris, *Chem. Eng. Sci.* **60**, 4749 (2005).
- [7] C. C. Yec and H. C. Zeng, *J. Mater. Chem. A* **2**, 4843 (2014).
- [8] I. M. Lifshitz and V. V. Slyozov, *J. Phys. Chem. Solids* **19**, 35 (1961).
- [9] P. W. Voorhees, *Annu. Rev. Mater. Sci.* **22**, 197 (1992).
- [10] P. t. Voorhees and M. Glicksman, *Acta Metall.* **32**, 2001 (1984).
- [11] P. Voorhees and M. Glicksman, *Metall. Mater. Trans. A* **15**, 1081 (1984).
- [12] A. Brailsford and P. Wynblatt, *Acta Metall.* **27**, 489 (1979).
- [13] J. Marqusee and J. Ross, *J. Chem. Phys.* **80**, 536 (1984).
- [14] Y. Enomoto, M. Tokuyama, and K. Kawasaki, *Acta Metall.* **34**, 2119 (1986).
- [15] V. M. Burlakov, *Phys. Rev. Lett.* **97**, 155703 (2006).
- [16] C. Beenakker and J. Ross, *J. Chem. Phys.* **83**, 4710 (1985).
- [17] G. Venzl, *Phys. Rev. A* **31**, 3431 (1985).
- [18] A. Chakrabarti, *Phys. Rev. Lett.* **69**, 1548 (1992).
- [19] D. W. Grunau, T. Lookman, S. Y. Chen, and A. S. Lapides, *Phys. Rev. Lett.* **71**, 4198 (1993).
- [20] Z. Huang, M. Su, Q. Yang, Z. Li, S. Chen, Y. Li, X. Zhou, F. Li, and Y. Song, *Nat. Commun.* **8**, 14110 (2017).
- [21] D. Yaron-Marcovich, I. Dror, and B. Berkowitz, *Chemosphere* **69**, 1593 (2007).
- [22] X. Zheng and J. Jang, *Sustainability* **8**, 1317 (2016).
- [23] S. S. Adkins, X. Chen, I. Chan, E. Torino, Q. P. Nguyen, A. W. Sanders, and K. P. Johnston, *Langmuir* **26**, 5335 (2010).
- [24] R. Anderson, L. Zhang, Y. Ding, M. Blanco, X. Bi, and D. P. Wilkinson, *J. Power Sources* **195**, 4531 (2010).
- [25] M. Buchgraber, A. R. Kovscek, and L. M. Castanier, *Transp. Porous Media* **95**, 647 (2012).
- [26] T. Xu, J. A. Apps, and K. Pruess, *Chem. Geol.* **217**, 295 (2005).
- [27] See Supplemental Material at <http://link.aps.org/supplemental/10.1103/PhysRevLett.119.264502> for thermodynamic data, which includes Refs. [28,29].
- [28] W. J. Lyman, W. F. Reehl, and D. H. Rosenblatt, *Handbook of Chemical Property Estimation Methods: Environmental Behavior of Organic Compounds* (American Chemical Society, Washington, DC, 1990).
- [29] R. Sander, *Atmos. Chem. Phys.* **15**, 4399 (2015).
- [30] K. Xu, T. Liang, P. Zhu, P. Qi, J. Lu, C. Huh, and M. Balhoff, *Lab Chip* **17**, 640 (2017).
- [31] K. Ma, R. Lontas, C. A. Conn, G. J. Hirasaki, and S. L. Biswal, *Soft Matter* **8**, 10669 (2012).
- [32] Z. Khatib, G. Hirasaki, and A. Falls, *SPE Reservoir Eng.* **3**, 919 (1988).
- [33] R. Lontas, K. Ma, G. J. Hirasaki, and S. L. Biswal, *Soft Matter* **9**, 10971 (2013).
- [34] A. Kovscek and C. Radke, *Colloids Surf. A* **117**, 55 (1996).
- [35] K. Xu, C. P. Tostado, J.-H. Xu, Y.-C. Lu, and G.-S. Luo, *Lab Chip* **14**, 1357 (2014).
- [36] J. Hornbrook, L. Castanier, and P. Pettit, in *SPE Annual Technical Conference and Exhibition* (Society of Petroleum Engineers, Dallas, TX, 1991).